UNIVERSITY OF CALIFORNIA,
IRVINE

Measurements of Water Flow Rate and Slip Length in Single Nanopipes

DISSERTATION

submitted in partial satisfaction of the requirements
for the degree of

MASTER OF SCIENCE

in Physics

by

David Joseph Mallin

Dissertation Committee:
Professor Peter Taborek, Chair
Professor Zuzanna Siwy
Professor Albert Siryaporn

2016

DEDICATION

For friends and family.

TABLE OF CONTENTS

LIST OF FIGURES

ACKNOWLEDGMENTS

I would like to thank Professor Taborek, Dr. Angel Velasco, Dr. Robert Joachim, Dr. Jefferey Botimer, Dr. Chin-Chang Kuo, and Virginia Mac. All scanning electron microscope images were taken at the Laboratory for Electron and X-Ray Instrumentation (LEXI).

ABSTRACT OF THE DISSERTATION

Measurements of Water Flow Rate and Slip Length in Single Nanopipes

By

David Joseph Mallin

Master of Science in Physics

University of California, Irvine, 2016

Professor Peter Taborek, Chair

We have experimentally measured flow rates of water through hydrophilic and hydrophobic single pipes with diameters ranging from 10 μm to 200 nm. We developed a method of coating the pipes with a hydrophobic polymer roughly 2 nm thick and verified the hydrophobic nature of the pipes after treatment. The exact diameters of the tubes were measured using a gaseous flow impedance test or imaged directly via scanning electron microscopy. The flow rates through both the hydrophobic and hydrophilic pipes agree with theory for viscous Poiseuille flow and are effectively indistinguishable from each other.

Chapter 1

Introduction: Concepts and Controversy

The no slip boundary condition for viscous flow defines the velocity profile in a pipe by forcing the velocity to be zero at the walls. This boundary condition predicts macroscopic flow rates, but does not originate from any fundamental principle. If this assumption is untrue, the molecules at the wall have nonzero and "slip" along the boundary. As a result, the velocity profile (and net flow rate) changes. There are several factors that have been theorized to affect slip, including surface roughness, hydrophobicity, and trapped nanobubbles[3, 13, 11]. The effects of hydrophobicity in particular have been studied intermittently since the 1800's [6]. The growth of microfluidics and nanofluidics devices in recent decades has produced an increased interest in slip, as the effects become more relevant at smaller length scales. Thus, determining the scale at which slip might occur could have implications for many fields, including biological systems, DNA sequencing, desalination, and refrigeration[7, 9, 10, 14, 17].

The current body of research concerning hydrophobic effects on slip includes many conflicting reports. Reports on slip length (which will be explained in the theory section) range from <10 nm[13] to tens of microns [11]. In particular, two studies, by Byun[3] and

Schaeffel[13], used the same hydrophobic material and found completely different results. Schaeffel et al. and Byun et al. both studied water flow in poldimethylsiloxane (PDMS) coated microchannels. Both groups also used photo image velocimetry (PIV) in order to determine the velocity field and subsequent flow rates. Schaeffel reported a slip length of less than 10 nm while Byun reported a slip length of 2 μm. This is a discrepancy of over three orders of magnitude, for which the cause is unclear. It is possible that the fabrication of the microchannel from multiple pieces or the tracer particles from the PIV affect the flow. In order to eliminate these possible sources of error, we present a technique to directly measure the flow rate through a single nanoscale tube.

Chapter 2

Theory: Poiseuille Flow and the No Slip Boundary Condition

2.1 Laminar Flow Through a Pipe

Laminar flow through a cylindrical pipe can be derived exactly from the Navier-Stokes equations in cylindrical coordinates. For laminar flow, the following assumptions are made:

1. The flow is in a steady state (all $\frac{\partial}{\partial t} = 0$)
2. The flow velocity is only in the z-direction ($u_r = u_\theta = 0$)
3. The flow is symmetric about the center (all $\frac{\partial}{\partial \theta} = 0$) and fully developed ($\frac{\partial u_z}{\partial z} = 0$)

Under these assumptions, the radial momentum equation yields $\frac{\partial p}{\partial r} = 0$, which means pressure will only vary in the z-direction (along the length of the pipe). The ϕ equation becomes trivially satisfied. The z momentum equation reduces to:

$$\frac{1}{r}\frac{\partial}{\partial r}\left(r\frac{\partial u_z}{\partial r}\right) = \frac{1}{\mu}\frac{\partial p}{\partial z}, \tag{2.1}$$

where μ is the dynamic viscosity and u_z is the velocity field in the z-direction. The solution to this differential equation is

$$u_z = \frac{r^2}{4\mu}\frac{\partial p}{\partial z} + c_1 \ln(r) + c_2. \tag{2.2}$$

The flow velocity cannot be infinite at r = 0, so $c_1 = 0$. Also, the pressure drop along the pipe is assumed to be linear, allowing $\frac{\partial p}{\partial z} = \frac{\Delta P}{L}$, where ΔP and L are the pressure drop across and length of the pipe.

The determination of c_2 is at the heart of this experiment. The value of c_2 determines the velocity of the fluid at the wall of the pipe. Traditionally, the no-slip boundary condition of $u_z = 0$ at r = R (radius of the pipe) has been applied. However this is not the only theoretically acceptable boundary condition. It is also possible and completely acceptable to have a non-zero velocity at the walls of the pipe, as the no-slip boundary condition has no theoretical basis. It is a purely phenomenological boundary condition that yields correct flow rates for macroscopic flows. The velocity used for $u_z \neq 0$ at r = R is

$$u_z(R) = b\frac{\partial u_z}{\partial r}, \tag{2.3}$$

where the velocity at the wall is proportional to the radial velocity gradient at the wall times a constant b, which is the slip length. The slip length has units of length as implied and represents the distance that the velocity profile extends past the physical wall of the pipe.

With the no-slip boundary condition, the parabolic velocity profile is

$$u_z = \frac{1}{4\mu}\frac{\Delta P}{L}(R^2 - r^2), \tag{2.4}$$

With slip allowed, the shifted parabolic velocity profile is

$$u_z = \frac{1}{4\mu}\frac{\Delta P}{L}(R^2 - r^2 + b\frac{\partial u_z}{\partial r}). \tag{2.5}$$

A representation of the difference in velocity profiles is provided in Figure 2.1. In order to

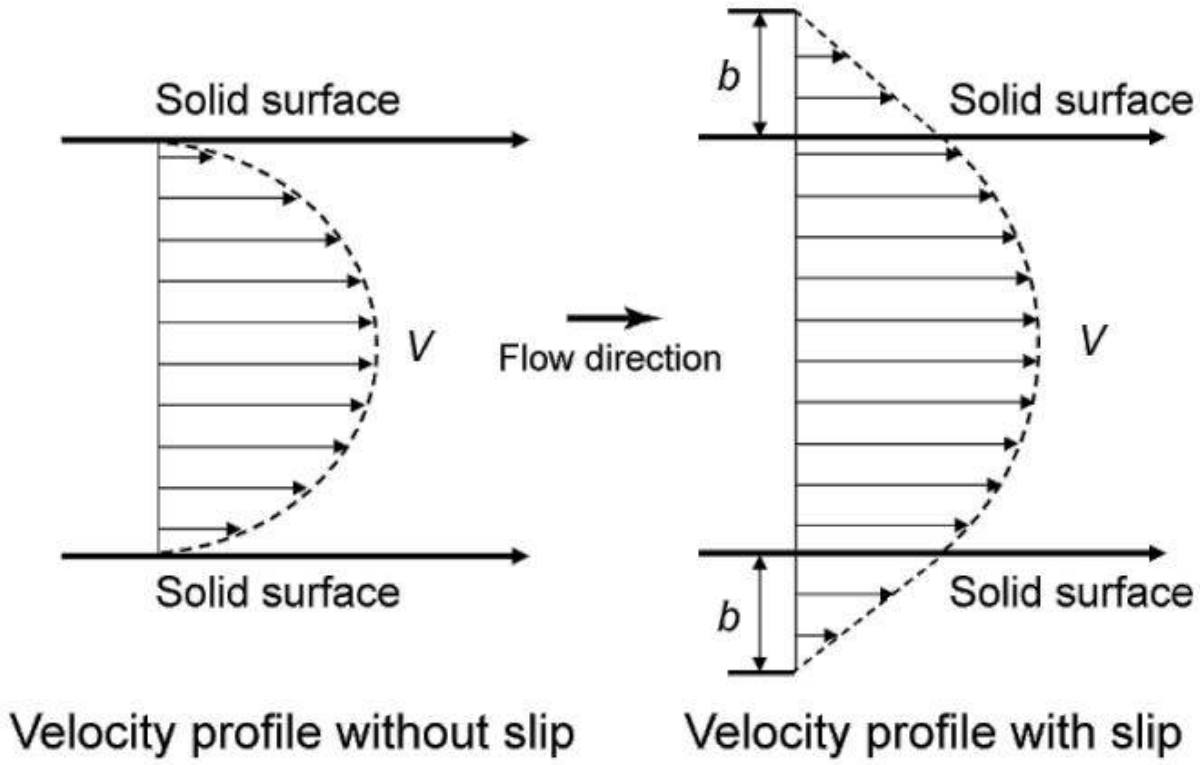

Figure 2.1: Cross sectional representations of no-slip and slip velocity profiles. The no-slip profile on the left shows a completely parabolic shape that reaches zero at the boundary. The slip profle on the right extends past the physical boundary by a slip length b. The velocity profile is linear after the boundary, taking on the slope of the tangential velocity at the boundary[1].

extract a net flow rate, the velocity is integrated over the area of the pipe. In the no-slip case, this yields the equation for Hagen-Poiseuille flow,

$$Q = \frac{\pi r^4 \Delta P}{8\mu L}, \tag{2.6}$$

where Q is the volumetric flow rate. If slip is allowed, we see an additional flow term:

$$Q = \frac{\pi \Delta P}{8\mu L}(r^4 + 4br^3). \tag{2.7}$$

For most macroscopic pipes, the normal contribution to the flow, proportional to r^4, far outweighs the slip contribution unless the slip length is of the order of the pipe size. A given slip length becomes more relevant (and thus easier to detect experimentally) as pipe size decreases.

2.1.1 Contact Angle

While the consequences of slip flow (increased flow rate) are easy to understand, the origin of the slip itself is still poorly understood. Research on the subject has not reached a consensus on the cause, and often reaches conflicting conclusions. The common proposed causes of slip include surface roughness, hydrophobicity, and trapped nanobubbles[3, 11, 13]. In our experiments, we focus on testing the effect of hydrophobicity on slip length.

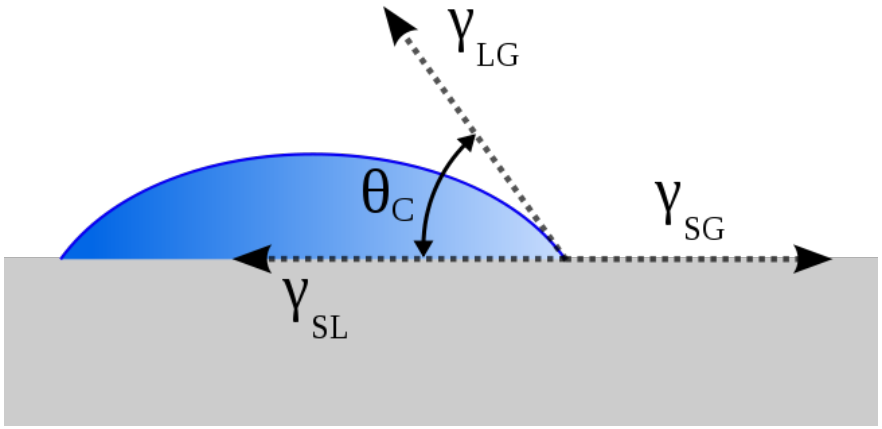

Figure 2.2: This contact angle diagram shows the relevant quantities in Young's equation, which controls the shape of the drop. The γ quantities refer to the interfacial energies between the different states and θ_c is the contact angle. If θ_c is greater than 90°, the surface is said to be hydrophobic, and if θ_c is less than 90°, the surface is said to be hydrophillic.

Contact angle is the common way to describe the degree of hydrophobicity. More generally, contact angle describes the wettability of a solid surface by a liquid. The relative interfacial energies of the gas, liquid, and solid dictate the shape of a drop of fluid on a solid surface. The relationship between these energies and the contact angle, shown in Figure 2.2,

is given by Young's equation,

$$\gamma_{SG} - \gamma_{SL} - \gamma_{LG} \cos\theta_c = 0. \tag{2.8}$$

where θ_c is the contact angle and the γ terms represent the interfacial energies of the solid-gas, solid-liquid, and liquid-gas interfaces. If the contact angle is greater than 90°, the surface is said to be hydrophobic, and if the contact angle is less than 90°, the surface is said to be hydrophillic.

The fused silica used in our experiments is naturally hydrophillic, but can be made hydrophobic via coating with a hydrophobic material, such as the polymer polydimethylsiloxane (PDMS). In simple terms, water interacts more strongly with the fused silica surface than the PDMS surface. The decreased surface interaction between PDMS and water might allow water molecules to violate the no-slip boundary condition.

Chapter 3

Direct Measurements of Water Flow through Single Nanopipes

The challenge of measuring fluid flow on the nanoscale is complex, and has been approached several different ways. Particle image velocimetry (PIV) is a common technique that involves seeding water with fluorescent tracer particles. The flow is then characterized by imaging the fluorescing particles[3, 13, 15]. By calculating the velocity of the particles in different sections of the flow, a velocity profile can be produced and from this a net flow rate. This technique has the advantage of measuring the velocity profile directly, but has a few disadvantages that led us to employ another method. First, it requires the construction a rectangular flow channel in order for the particles to be imaged. The construction of such a channel usually employs etching processes to create an open channel which is then closed by bonding a flat, transparent cover (often a simple microscope slide). The nature of the construction leads to questions of the uniformity of the channel and possible deformation under pressure(typical pressures for nanoflows can reach 50 atm). The other problem with PIV is the particle tracers that are employed. The particles themselves can be hundreds of nanometers or micron sized, giving them a non-negligible effect on the flow. There is essentially a lower limit on the channel size before the tracers become significant.

There are other methods as well, including using interferometry[5] or imaging[15] to measure the speed of a moving meniscus, using massive arrays of tubes and simply dividing a macroscopic flow by the number of tubes[11], or using a mass spectrometer[16]. Ideally, a direct measurement of the flow is made through a single tube. We perform such a measurement on successively smaller tubes from 10 μm to 200 nm. For previously stated reasons, the smallest tubes yield the most information on the no-slip boundary condition. Therefore, all the following procedural details are be told in the context of working with 200 nm tubes.

3.1 Measurement of Nanoscale Water Flow through Single Pipes

The basic concept of our experiment is to image a water droplet growing on the end of a nanotube over time. A pressurized water reservoir is attached to one end of the nanotube. Water flows out of the other side and into a reservoir of viscous oil. The water creates a bubble on the end of the tube that grows over time. The bubble is periodically imaged and those images are processed to extract the volume. The volume as a function of time yields flow rate. A basic diagram is show in Figure 3.1.

3.1.1 The Nanotubes

We acquired fused silica capillary tubing from Polymicro Technologies®. They produce high purity fused silica capillary tubing whose inner diameter can range from 2 mm down to 200 nm. The process of heating and pulling the capillary tubing leaves the inner surfaces clean, smooth, and chemically inert. This makes them ideal for flowing water through unaltered pipes, as well as for coating. The capillary tubing outer diameter is typically 125 μm or 350 μm, making them easy to handle. A yellowish brown polyimide coating supports and protects the fused silica.

When we acquire the tubing, which comes in a 10 m spool, we are given a diameter

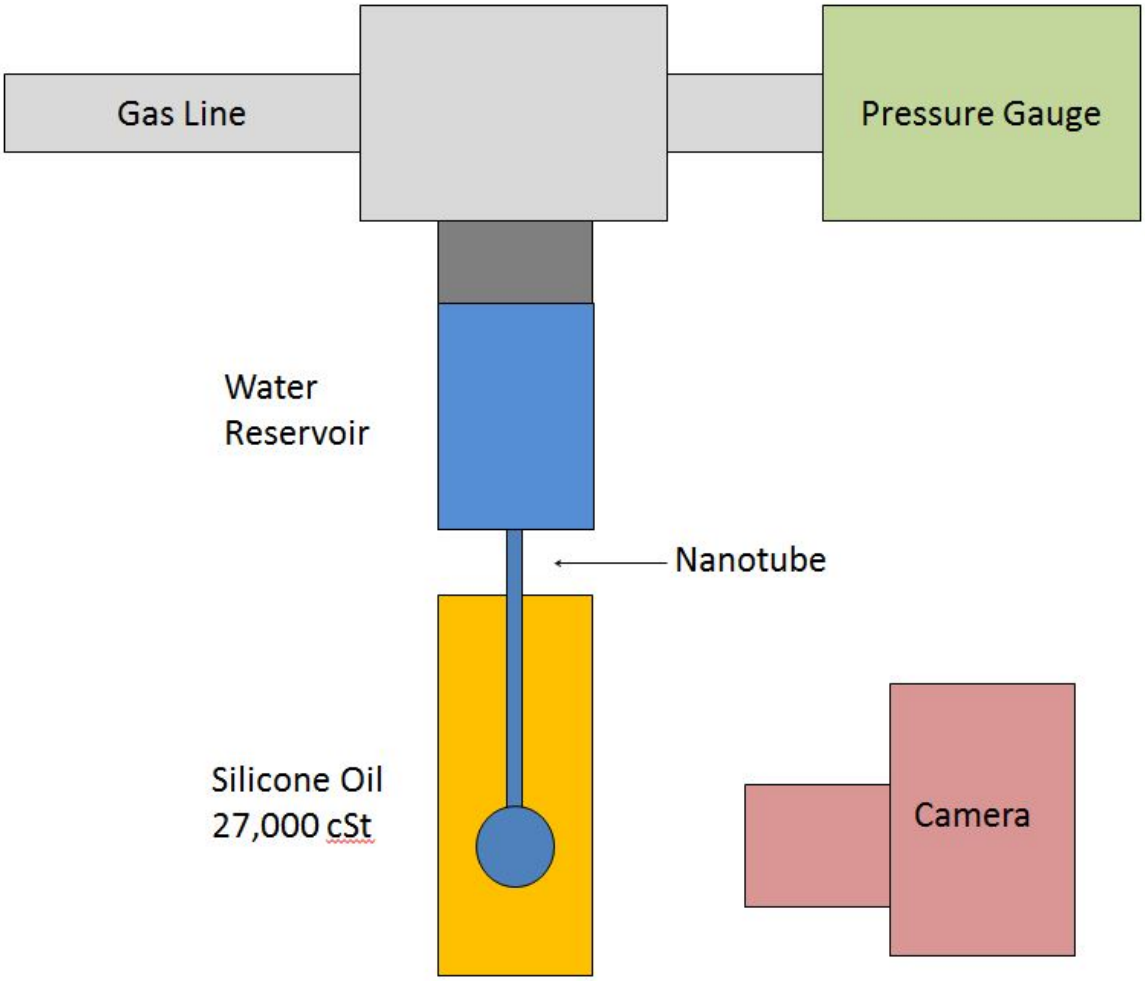

Figure 3.1: A diagram of the experimental setup.

for the beginning and the end, which Polymicro Technologies® determined via scanning electron microscopy (SEM). The diameter of the tube is effectively constant over the length of a single tube for our experiment (roughly 25 mm), but can vary over longer lengths. This requires us to determine the tube diameter after each experimental run. Depending on the nominal tube size, this was accomplished in one of two ways. For larger tubes (greater than 2 μm), we use a mass spectrometer technique to measure gas flow of helium through the tube. The technique is one our lab commonly employs and is described by Velasco[16]. For small tubes, we image the ends of the tubes via SEM. The fused silica nanotubes must be coated with metal before being imaged in an SEM. Both the metal coating and imaging are

carried out at the Laboratory for Electron and X-Ray Instrumentation (LEXI) user facility. A South Bay Technology Ion Beam Sputter Deposition and Etching System Model IBS/e is used to sputter roughly 2.5 nm of iridium onto the end of the tube. The angle and rotation of the coating process means that the diameter of the tube is effectively unchanged by this coating. The tube is then imaged in a FEI Magellan 400 XHR SEM. Figure 3.2 shows the entire end of the tube. Several images similar to Figure 3.3 of the inner diameter are taken. For each image, 20-30 points are taken around the circumference of the hole and fit to a circle profile in Mathematica. The resultant diameters from the fits are averaged for the final diameter used to compare to the water flow data. Typically, the diameters calculated from separate SEM pictures are within 2 nm of each other.

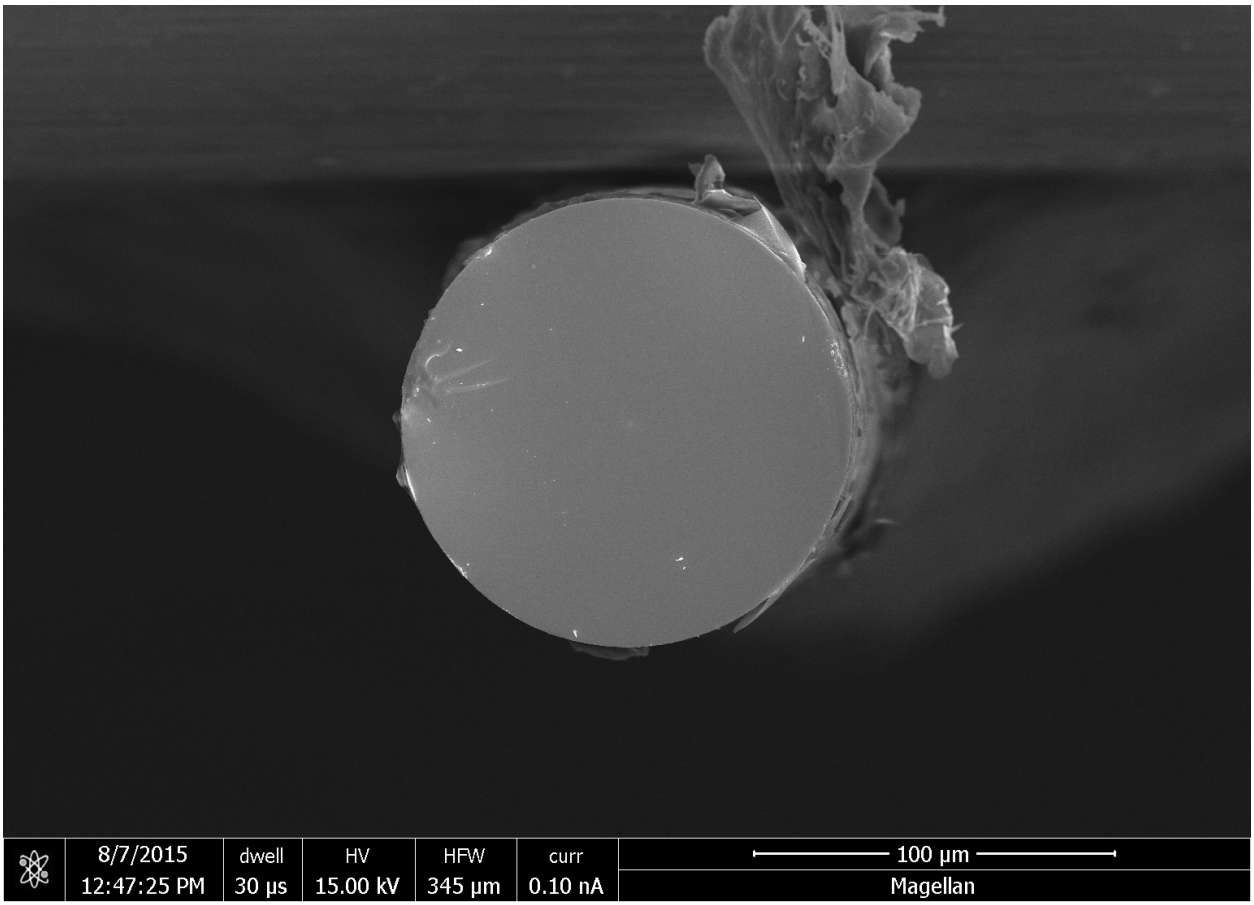

Figure 3.2: SEM image of the 200 nm inner diameter nanotube tip, coated in 2.5 nm of iridium. To give an idea of the scale, the 200 nm inner diameter can barely be seen in the center. The success of the cleave is shown by the smoothness of the face surface, showing only small imperfections where the diamond scribe nicked the edges.

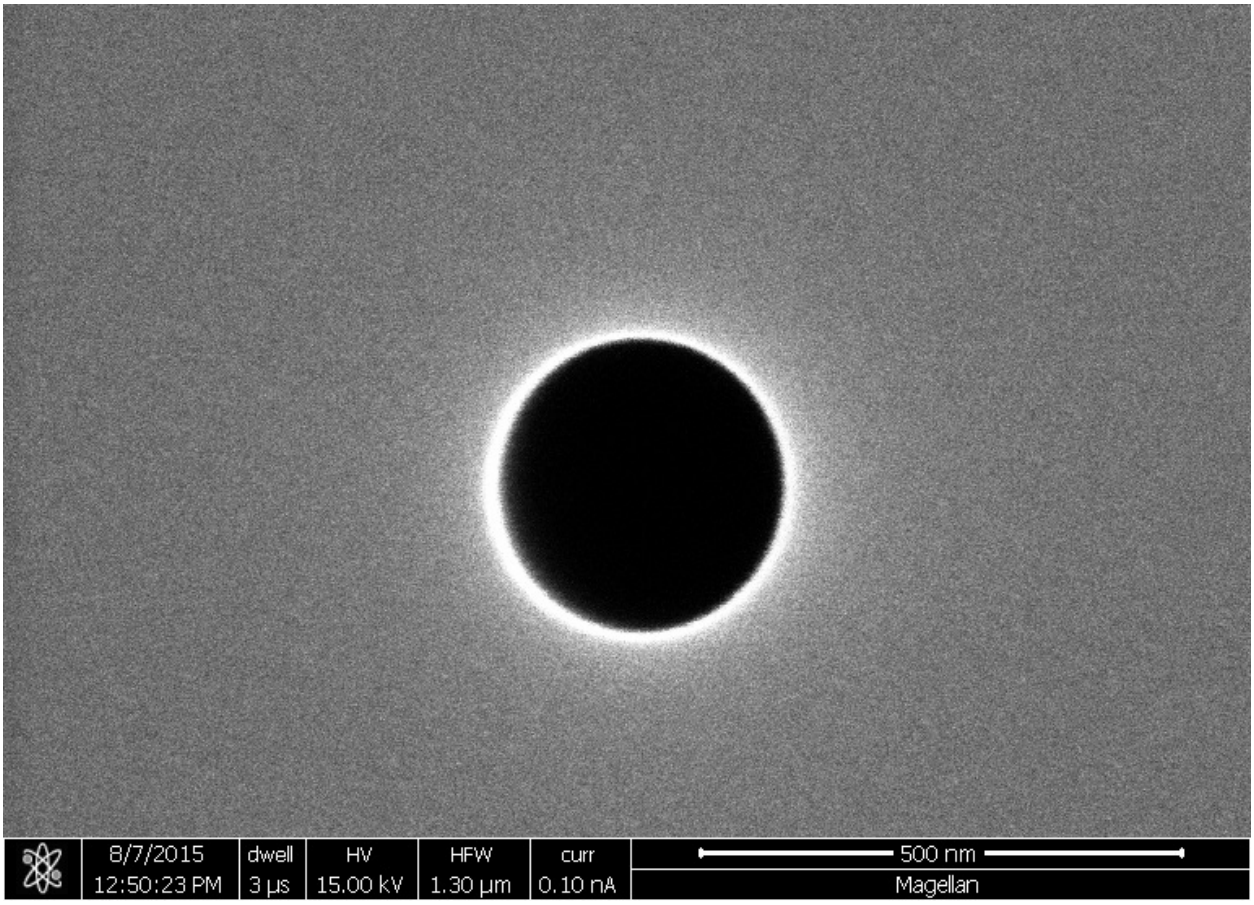

Figure 3.3: SEM image of the inner diameter of a 200 nm uncoated nanotube. The brightness in the center is a charging effect due to the iridium coating not penetrating down the tube. Several images such as this one are taken for single tube, and the average of the calculated diameter is used

There are several steps to preparing a nanotube for the experiment. The first is to separate a section of tubing from the spool. This is performed by scoring the tubing with a diamond scribe. It is important that the diamond scribe penetrates through the polyimide coating, but just barely scratches the fused silica. Once the silica is scored, pulling along the length of the tube causes it to break very cleanly. This is important since our experiment relies on the fact that the drop on the end of the tube is spherical(there is a correction that takes place in the image processing). If the tube face is not flat, the drop is misshapen and the volume cannot be calculated properly. This is an arduous process and one attempt in five is usually successful. The face is visually inspected under a microscope at 50x magnification to

ensure the pipe was cleaved properly. In order to do this inspection, the polyimide coating near the tip must be removed, as is sometimes obscures or extends past the tip. This is accomplished by burning the coating off with a propane torch. Care is taken to burn the coating off without melting and deforming the fused silica.

After the tube is cleaved and inspected, is it epoxied into a 1/4" Swagelock VCR gland. The gland itself is a custom piece drilled out in two stages from a blank. A large bit around 3/8" is used to drill most of the way through, leaving roughly 1/4". This section forms the water reservoir for the flow. A smaller, 1/16" drill is used to break through. The tube is epoxied into this smaller hole. The two-stage shape helps the epoxy form a "plug" that prevents leaks. The smaller secondary hole also decreases the force on the epoxy, since pressures can reach up to 50 atm. We use Stycast 2850FT as an epoxy along with the 23LV catalyst. The epoxy is generally known for its uses at very low temperatures, but it works well here too. It is also very resistant to solvents, which means that the epoxy plug must be removed with a drill experimental between runs.

The VCR gland is pressurized by attaching a tank of Ultra High Purity Helium (99.995%) supplied by Airgas. Helium is chosen for its very low solubility in water and chemical inertness. The pressure on this side is measured with an Omega Engineering®PX309-1KG5V pressure gauge with a 17V excitation. It is important that the tube is pressurized and has flowing water before the oil reservoir is raised to insert the tube. This prevents the oil from pushing into and clogging the tube.

3.1.2 The Hydrophobic Coating

In order to test the effects of contact angle on flow rate, both hydrophilic and hydrophobic nanotubes are required. Untreated tubes are naturally hydrophilic. They must be treated to be made hydrophobic. The first attempt to make the tubes hydrophobic used octadecyltrichlorosilane (OTS), an organometallic chemical that can produce a hydrophobic monolayer. The process involved cleaning the silica surfaces to be coated with acid in order

to expose hydroxyl groups to which the OTS can bond. For the nanotubes, this means flowing strong acid through the tubes at high pressure (in order to achieve acceptable flow rates). This coating process also requires a dry nitrogen environment, as OTS reacts with water. Several attempts yielded tubes through which there was no flow. We believe this to be due to water vapor contamination.

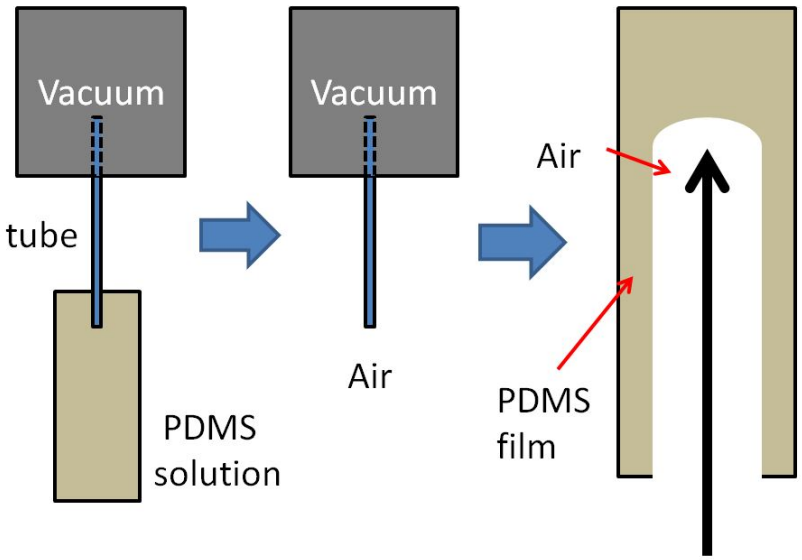

Figure 3.4: A diagram of the coating process. One end of a tube is dipped into a solution of PDMS and cyclohexane while the other end is exposed to vacuum. Then the tube is removed from the solution and exposed to air while the other remains under vacuum. An air bubble travels up the tube, leaving a thin PDMS film behind.

Coating the tubes with OTS was abandoned in favor of poldimethylsiloxane (PDMS), even though OTS has a greater contact angle (110°)[8] than that of PDMS (105°)[3, 13]. The coating method was inspired by Chen[4] and Bretherton[2] studying the film thickness around a bubble that travels through in a capillary. The idea is to fill the capillary with the desired liquid coating. Then, simply force an air bubble to travel the pipe, leaving a thin film. A diagram of the process is hown in Figure . The PDMS we use is Sylgard 186, which comes as two parts and has a high viscosity of 66.7 Pa·s. In order to achieve a thin coat of PDMS, the mixture is diluted 10:1 by mass with cyclohexane. Tubes roughly 10 cm long are fixed into a PDMS cap, with one side exposed to vacuum from a rotary vane pump and the

other immersed in the PDMS-cyclohexane solution. The previously mentioned polyimide coating is removed prior to coating. This ensures that the high temperatures involved in removing the polyimide does not affect the PDMS. The tubes stay immersed for roughly 20 minutes, which allows for the solution in the tube to be refreshed multiple times. The immersed end is then removed and exposed to air, allowing for a film to be created as the air passes through the tube. The tubes are then baked for one hour at 100°C. The thickness of the coating immediately after is estimated by[4]:

$$h = 1.337\ r\left(\frac{\mu\ v}{\gamma}\right)^{\frac{2}{3}}, \tag{3.1}$$

where r is the radius of the pipe, μ is the dynamic viscosity of the fluid, v is the velocity of the bubble, and γ is the interfacial surface energy. For the diluted PDMS in a 200 nm fused silica pipe, we calculate the coating to be 20 nm thick before curing. The combination of the cyclohexane evaporation and curing reduces the thickness to under 2 nm.

On a flat surface, hydrophobicity is easily verified by measuring the contact angle. For PDMS, the contact angle with water has been well documented to be 105°[3, 13]. For a tube, especially a very small tube, it becomes a nontrivial matter. Several methods are used to verify the existence of the coating, depending on the tube size. All three methods rely on the concept of capillary action. If a tube is hydrophillic, it is energetically favorable for water to be in contact with the surface. If a tube diameter is small enough, this can manifest in water filling the tube upwards against gravity until it reaches a height in which the increase in gravitational energy equals the decrease in surface energy. The height at which this equilibrium occurs depends on the size of the tube, surface tension, and contact angle. For water and tubes 10 μm in diameter and smaller, this height is on the order of meters. If a tube is hydrophobic, it is energetically unfavorable for water to be in contact with the tube surface. Water resists filling a hydrophobic tube until it is forced by an external pressure. The difference in behavior between hydrophilic and hydrophobic tubes makes it possible to

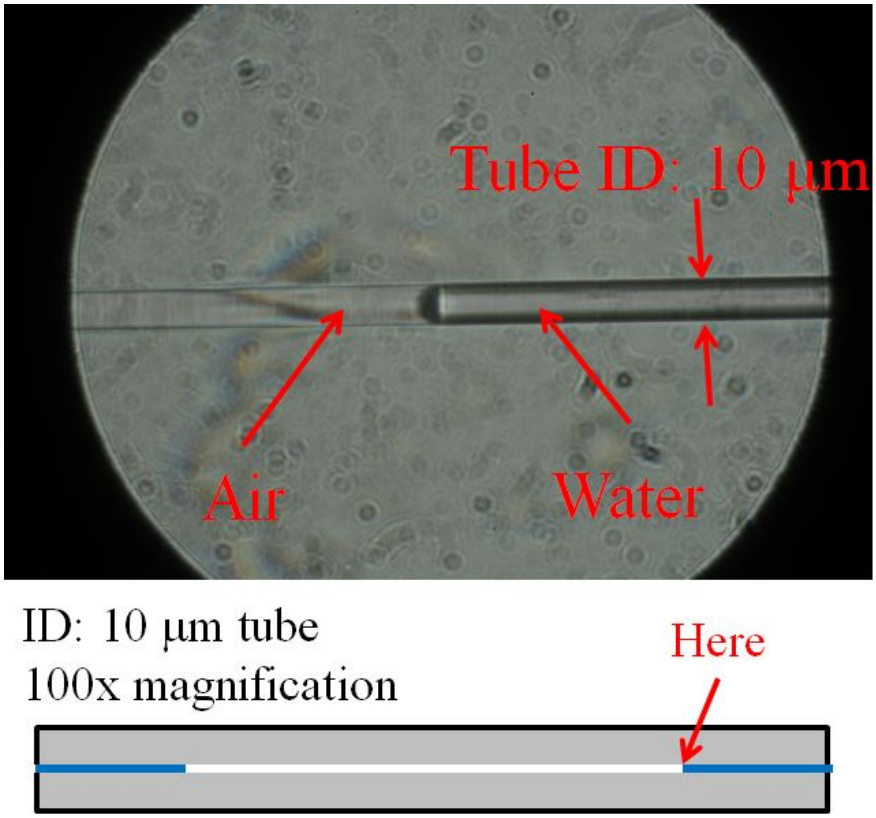

Figure 3.5: The observation of a meniscus inside a 10 μm tube confirms the hydrophobic condition of the tube and success of the coating process. The picture taken through a microscope objective shows the meniscus on the right side of the tube. To the right of the meniscus is water, while air is to the left. If the tube was hydrophilic, it would have completely filled with water.

verify the existence of the hydrophobic coating.

For large tubes (5 μm or larger), a meniscus can be viewed directly in a tube that is submersed in water. This is shown in Figure 3.5. A hydrophilic tube that is submersed in water will be filled. A hydrohpobic tube resists filling up to a certain depth (and consequent pressure) , and then begins to fill from both ends. However, the filling compresses the gas remaining inside the tube and reduces the net pressure. This allows for a static meniscus to exist within the tube whose location will change based on the depth.

For medium tubes (1 μm or larger), fluorescence imaging is used. The tips of both coated and uncoated tubes are immersed in a saturated solution of Rhodamine 610 perchlorate in water. Rhodamine 610 absorbs light at a wavelength of 543.02 nm and emits light

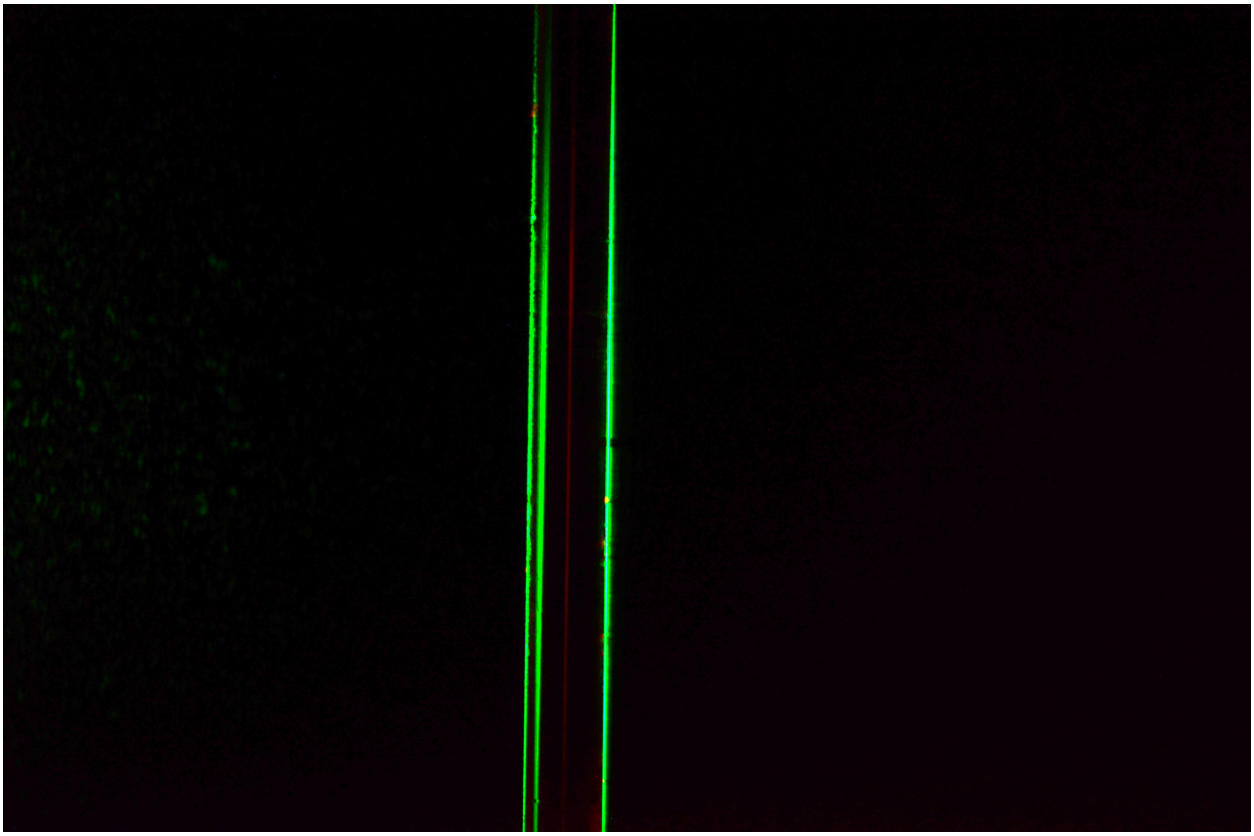

Figure 3.6: Example of fluorescence in a 2 μm tube. The orange colored center stripe is the fluorescence from the saturated Rhodamine 610 solution. The green stripes are lensed laser light from the pump.

at a wavelength 0f 610 nm. A diagram of the setup is shown in Figure .Both sets of tubes are dipped into the solution and imaged while being illuminated by a green laser at 532 nm. The uncoated tubes are hydrophilic, and should automatically fill with solution when they are dipped. The PDMS coated tubes should be hydrophobic and stay empty. The green laser light will pass through the coated tubes, while orange fluorescence is only seen in the uncoated tubes. The pictures are taken through two Thorlabs® FGL600 Longpass color filters which allows the orange fluorescence to be imaged while severely reducing the green laser light from the pump. An example of the tube fluorescence can be seen in Figure 3.6. The example shows that a substantial amount of laser light is bent towards the camera and penetrates the two filters. At 2 μm, it can be seen that the unwanted green light making it through the filters is brighter than the fluorescence. The fluorescence signal is proportional

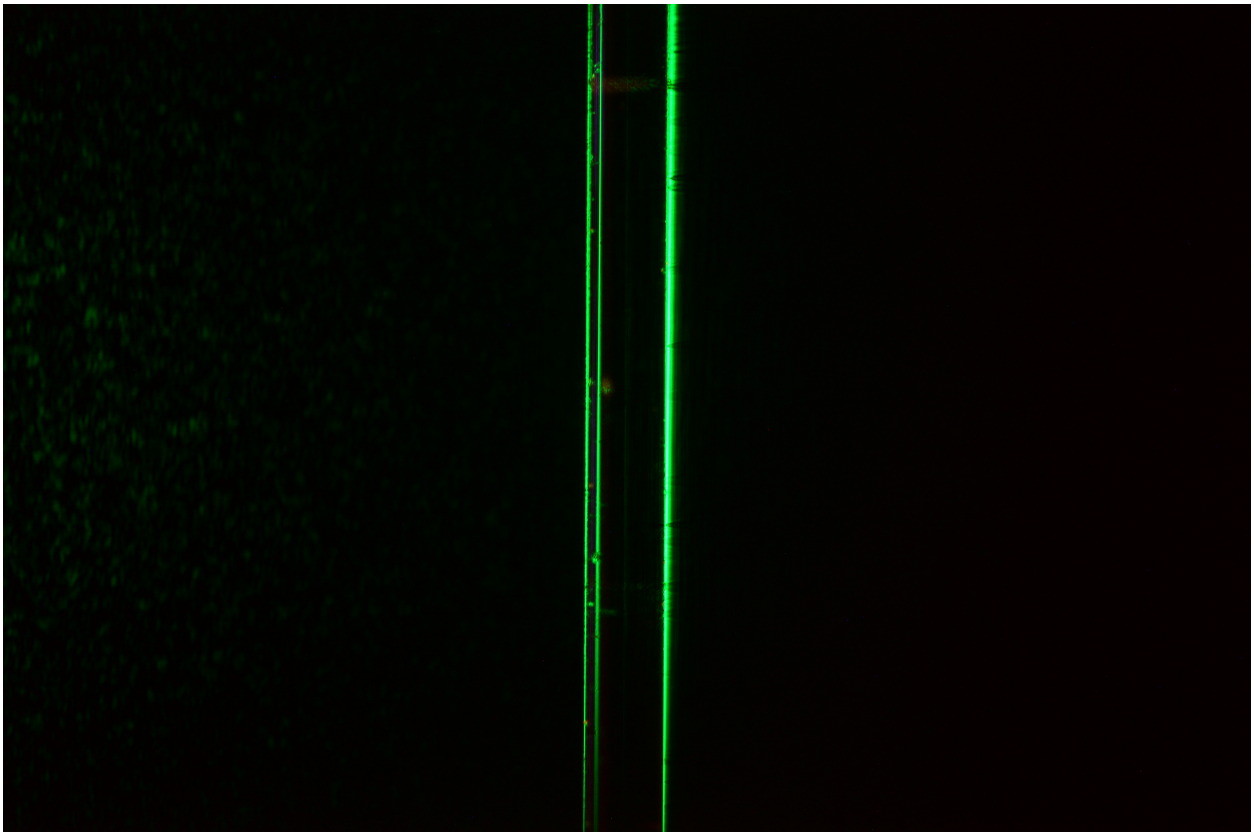

Figure 3.7: Any fluorescence signal is lost in the noise of the green pump laser, seen in the center of the tube.

to the volume, so it scales inversely with r^2. For nanometer sized pipes, the green light that is bent by the inner diameter masks any fluorescence that may be taking place. This can be seen in Figure 3.7.

For tubes with diameters less than 500 nm, the coating is verified by observing the difference in pressure required to begin flow. Figure 3.8 shows the qualitative flow behavior for hydrophobic and hydrophilic tubes as a function of external pressure drop. The flow for uncoated tubes begins with any pressure drop and increases linearly with pressure. For hydrophobic tubes, the external pressure drop must first overcome the negative capillary pressure before flow will begin. Once the threshold is reached, the behavior will be the same as the hydrophillic tube(assuming no slip). A qualitative graph of this behavior is shown in Figure 3.8. This is due to the Young-Laplace pressure of the interface, given by $\Delta P = \frac{2\gamma \cos\theta}{a}$, where γ is the surface tension, θ is contact angle, and a is the radius of the

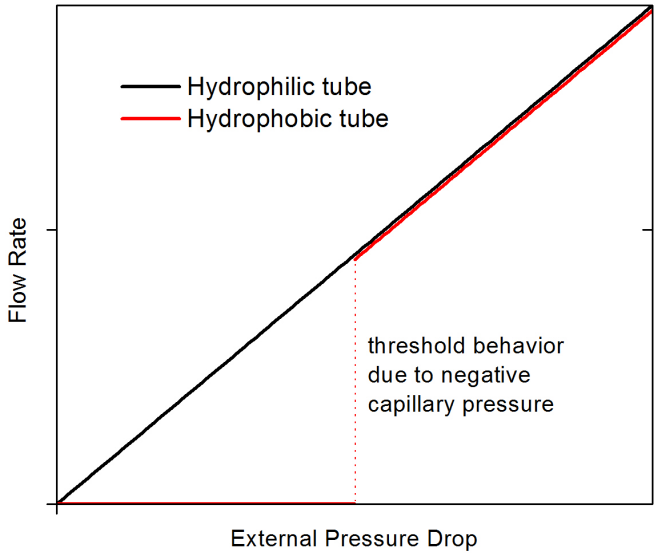

Figure 3.8: The theoretical flow behavior of a hydrophobic and hydrophilic tube as a function of external pressure drop differ due to capillary pressure. The hydrophobic tube negates any external pressure drop until a certain threshold, after which it adopts the same behavior as the hydrophilic tube(assuming no slip).

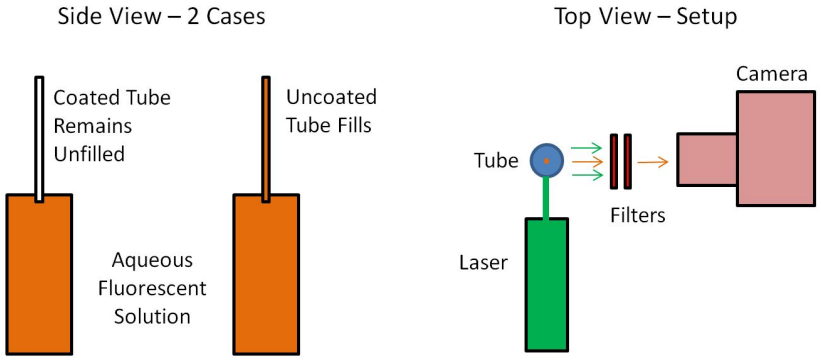

Figure 3.9: The setup used to verify the existence of the hydrophobic coating in 2 μm tubes relies on imaging of fluorescent dye in water. When the ends of the uncoated and PDMS coated tubes are dipped in fluorescent solution, only the uncoated tubes fills. Then, both tubes are illuminated with laser light, causing the solution in the uncoated tube to fluoresce. The light from the tube is filtered to remove the laser light before being captured by a camera oriented perpendicular to the laser.

pipe. For a 200 nm tube, it requires 3.72 atm to cause water to flow through the pipe. The coating is verified by observing the pressure-threshold behavior of the flow in the coated

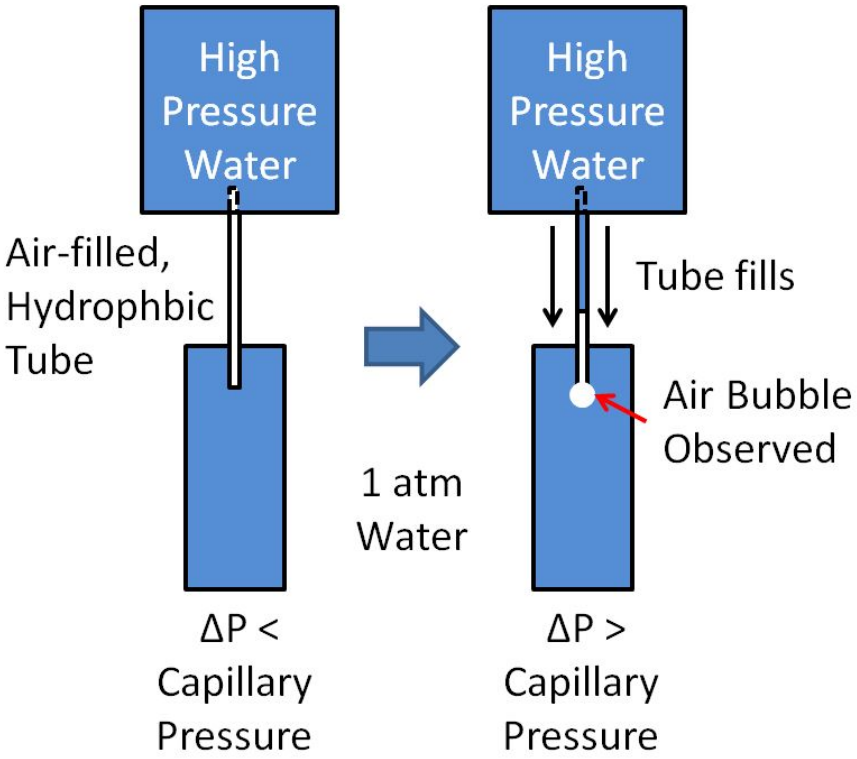

Figure 3.10: The coating in the 200 nm diameter tubes is verified be observing the threshold behavior of the flow with pressure. No flow is observed through an air-filled coated tube until the external pressure drop is enough to overcome the negative capillary pressure. Once this pressure is reached, the remaining air in the tube is pushed out and observed on the end of the tube.

pipes. This is accomplished by raising the reservoir pressure of the tube while the other tip of the tube is placed in water instead of oil. When the Young-Laplace pressure is overcome, the water flow pushes the remaining air out of the tube, and the bubble is observed. A diagram of this is shown in Figure 3.10.

3.1.3 The Water and the Oil

There are two liquids of importance in this experiment. The first is the water flowing through the nanotube. We use water filtered by an EMD Milipore Synergy R®. A drop of bleach is added to 500 mL of the filtered water to prevent bacterial growth. This step was added after observing flow rates reduce and eventually stop at around 10 hours of flow.

Research into biofilms in microchannels[12] led us to believe bacterial growth was the cause. Adding this step allows for continuous flows greater than several weeks. This in turn allows us to use our smallest tubes. The mixture was tested to ensure the contact angle with PDMS remained unchanged.

The second liquid of importance in the experiment is the silicone oil in which the water forms a drop. The water cannot simply form on the end of the pipe and be exposed to air. At the operating flow rates of this experiment, the water would evaporate as it flows through, rather than forming a drop. A viscous oil with low water diffusivity is used to contain the droplet. We use Cannon® N5100 Viscosity Standard, which has a density 0.883g/mL. The lower density of the oil causes drops that are removed from the tube tip to sink out of the way. The density difference combined with gravity can cause deformation in larger drops from a spherical shape to a teardrop shape. To determine whether this effect is important, we look at the capillary length. If the largest dimension of the system (in this case the diameter of the drop) is smaller than the capillary length, the drop will remain spherical in shape. The capillary length is given by $\lambda_c = \sqrt{\frac{\gamma}{\rho g}}$, where γ is the surface tension between the two fluids, ρ is the density of the fluid in question, and g is gravitational acceleration. For this system, the capillary length is about 2.2 mm. The drops in the experiment have a maximum diameter of 1 mm, meaning the spherical approximation holds.

3.1.4 The Pictures

The pictures of the drops are taken with a Nikon® D7000 DSLR camera, in combination with an Olympus® LMPlanFL 10x microscope objective. A sample picture is shown in Figure 3.11. The camera is set to take a picture every two hours. The flow is on the order of picoliters per second and a single drop can take up to 120 hours to form. The image processing relies on us being able to discern a difference in the radius from one picture to the next. Depending on the flow rate, we may only process every other picture.

The outer diameter of the nanotube is used as a calibration for the pixel to distance

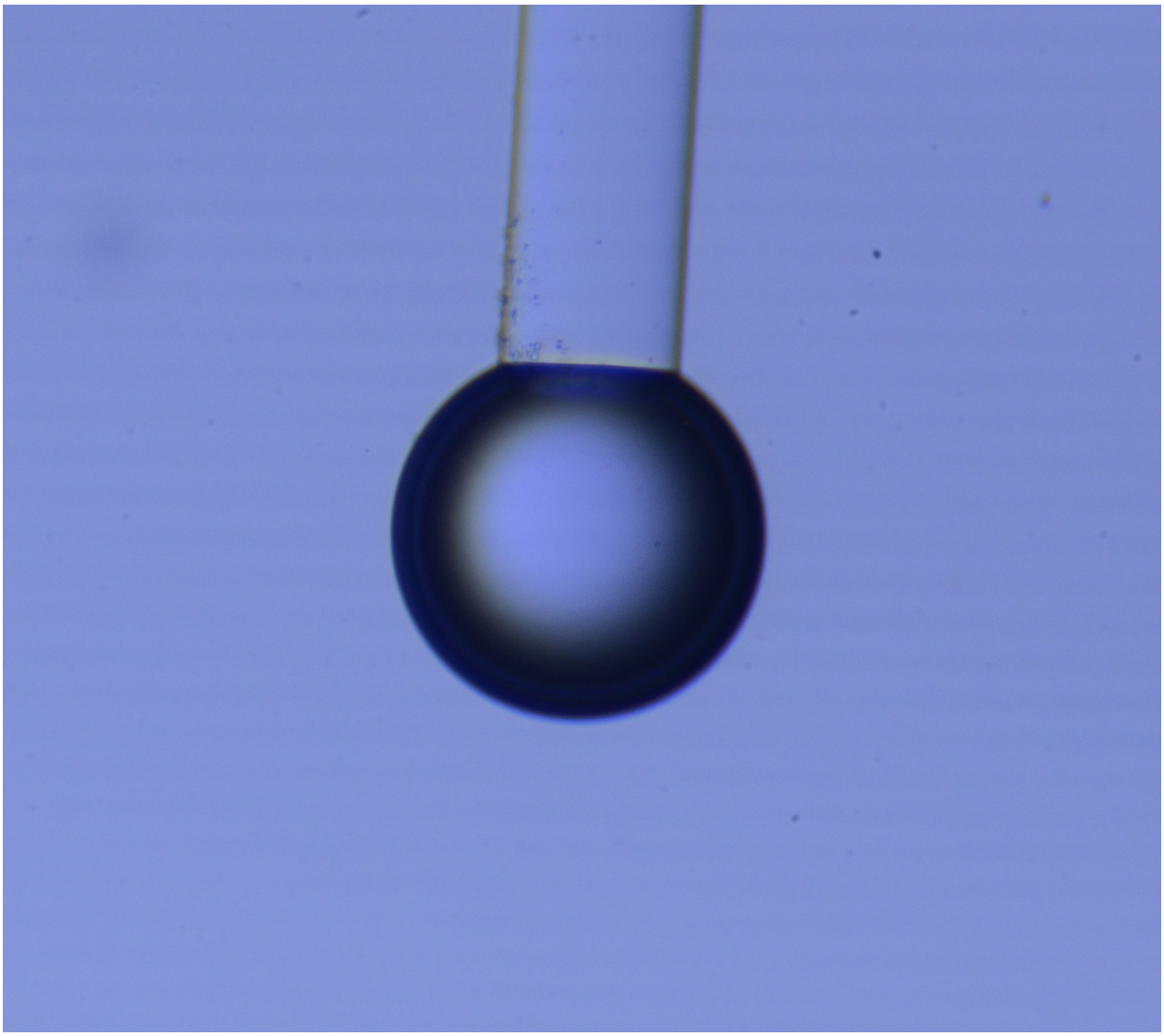

Figure 3.11: Sample of a drop picture. The picture was taken after 196 hours of flow through a 274 nm tube, with a pressure drop of 46.5 atm. The volume of this drop is 11.2 nanoliters.

conversion. The actual value is known from the same SEM imaging used to determine the inner diameter. The pixel diameter of the tube needs to be corrected for any tilt. Three points are taken from the picture, two on the left edge (A and B), and one on the right edge of the outer diameter (C). The perpendicular pixel distance is given by $\left|\frac{\vec{AB}}{|\vec{AB}|} \times \vec{AC}\right|$.

For each picture, roughly 20 pixel points are taken along the outer edge of the drop. These points are fit to a circular profile, and the radius and subsequent volume are calculated. This is not the final volume, as a correction must be made for the volume missing from the

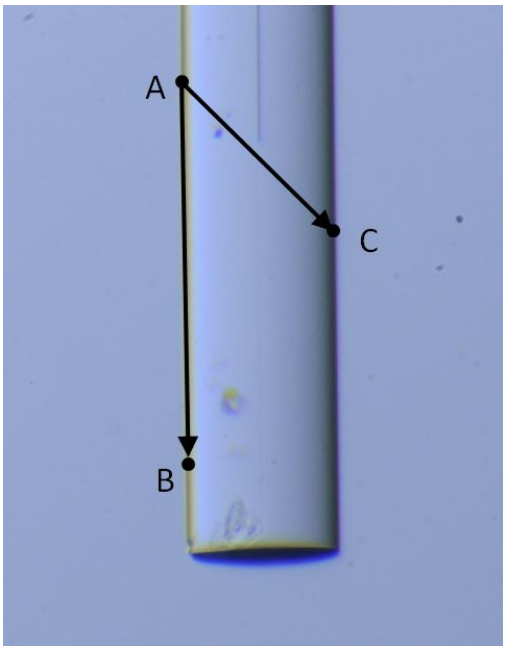

Figure 3.12: Diagram of the constructed vectors for the pixel to length calibration.

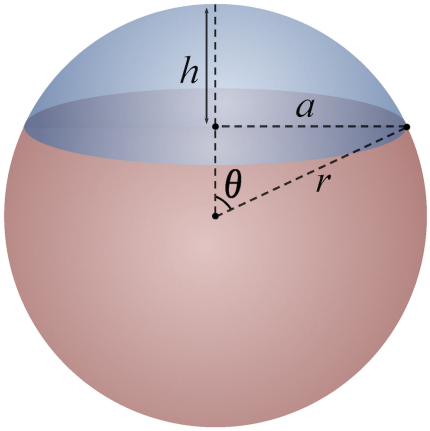

Figure 3.13: Diagram of the relevant parameters for the volume of a spherical cap.

"cap" of the drop where it comes into contact with the tube. The volume of a spherical cap is given by $V = \frac{\pi h}{6}(3a^2 + h^2)$, where a and h can be seen in Figure 3.13. The cap volume is subtracted from that of the sphere to give the total drop volume. The data of the drop volume over time is given a linear fit, where the slope of the fit is the flow rate.

Chapter 4

200 nm Indistinguishable Flows

Flow rates and slip lengths were measured through uncoated and PDMS coated tubes with diameters of 10 μm, 2 μm, and 200 nm for several pressures. The experiments are conducted in order of decreasing tube diameter. As diameter decreases, the experiment becomes increasingly sensitive to slip. The ratio of slip flow to no-slip flow is $\frac{4br^3}{r^4} = \frac{4b}{r}$, where b is the slip length. The capability to detect a 5% deviation in flow rate at each size would correspond to a specific slip length sensitivity. It is a slip length of 625 nm for 10 μm tubes, 12.5 nm for 2 μm tubes, and 1.25 nm for 200 nm tubes. The 200 nm tubes give the best sensitivity to slip, but the flow is much harder to measure experimentally. The larger tubes served to give and upper bound to the slip length value as well as provide experience and insight for the smaller tubes. They also hold the advantage of short trial runs (hours compared to days or weeks), which allowed for quick diagnosis and resolution of experimental challenges.

4.1 10 μm Data

Flows are measured through the tubes at room temperature with pressure drops ranging from 0.5 atm to 2 atm. Typical flow rates for 10 μm tubes are on the order of hundreds of nanoliters per minute. The first trials showed flow rates that follow theory at the beginning,

but then reduced after 2-4 hours. This is unacceptable for trial runs in tubes smaller than 10 μm that require longer time (multiple days or weeks). The culprit for the reduced flow was found in bacterial growth, after reading about biofilm production in laminar flows in microchannels[12]. A simple solution to the problem was implemented in the form of adding a small amount of bleach (roughly 200 ppm) to the milipore water used for the experiment. The maximum time for flows is increased from a few hours to 2+ weeks. This allowed for longer experimental runs as well as multiple runs at different pressures on a single tube. Figure 4.1 shows the difference in a typical 10 μm flow run with and without bleach added to the water.

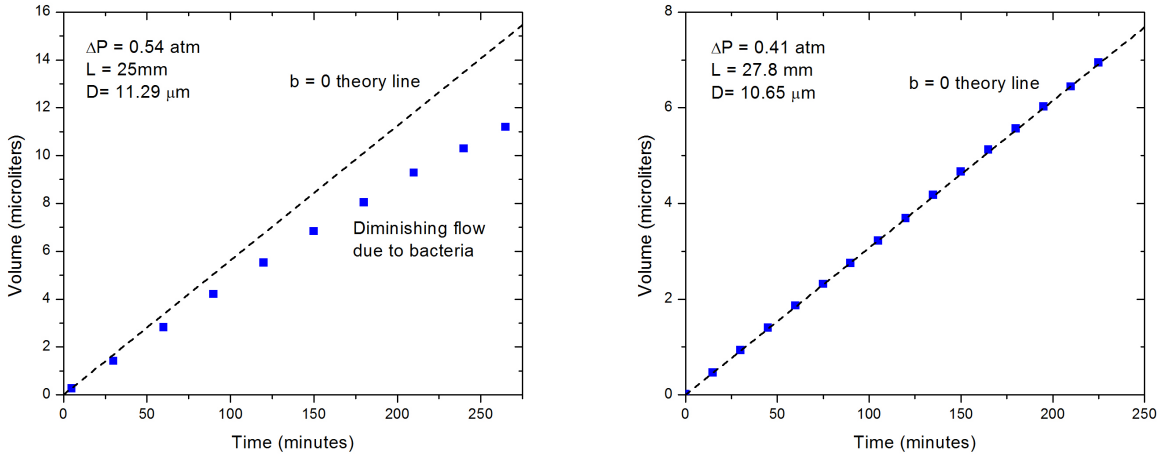

(a) Flow run without bleach.

(b) Flow run with bleach.

Figure 4.1: Flow runs through 10 μm diameter tubes, one with pure milipore water and the other with bleach added to the milipore water to inhibit bacterial growth. This measure increased the maximum time for a flow run from a few hours to 2+ weeks.

Investigations into pressure drop dependence were performed at the 10 μm diameter level as well. Figure 4.2 shows multiple flow runs through a single coated tube at several pressures. The data follows the no-slip theory closely for all three pressures, with no trend in slip length with pressure.

The flow data between uncoated and PDMS coated 10 μm tubes was indistinguishable within a slip length of 100 nm. There is also no discernible dependence in the measured slip

on pressure. In order to investigate slip lengths shorter than 100 nm, smaller tubes were used.

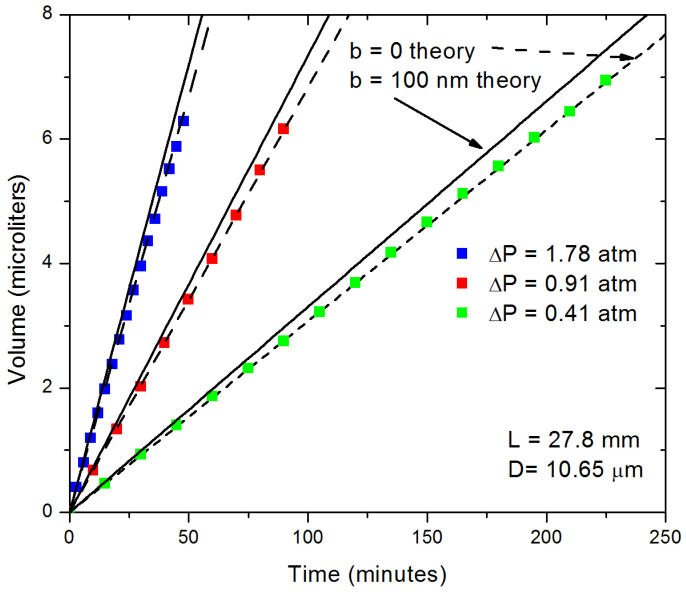

Figure 4.2: Flow data through a PDMS coated, 27.8 mm long, 10.65 μm diameter tube for pressure drops of 0.41 atm, 0.91 atm, and 1.78 atm. The measured flow rates for this tube yield slip length values of less than $\pm$ 10 nm.

4.2 2 μm Data

Flow data and slip measurement in 2 μm diameter tubes were performed with the methods and techniques learned from the 10 μm tubes. The pressure drops for the 2 μm flow data ranged from 1.5 to 5 atm, with typical flow rates on the order of nanoliters per minute. The 2 μm graph in Figure 4.3 visually shows higher deviation between the flow data and the theory than the 10 μm graph. This is because the 2 μm tubes are five times more sensitive than the 10 μm tubes. Small deviations from theory begin to appear much larger as tube diameter decreases. The average coated slip length (58 nm) and the average uncoated slip length (87 nm) differ by only 29 nm. This was roughly the same as the range

of slip values that was commonly measured in a single tube (26 nm for the uncoated data shown). Therefore, it is not possible to tell if the difference is actually due to slip. It can be concluded from this data that the flow through the 2 μm coated and uncoated tubes is indistinguishable to within a slip length of 30 nm.

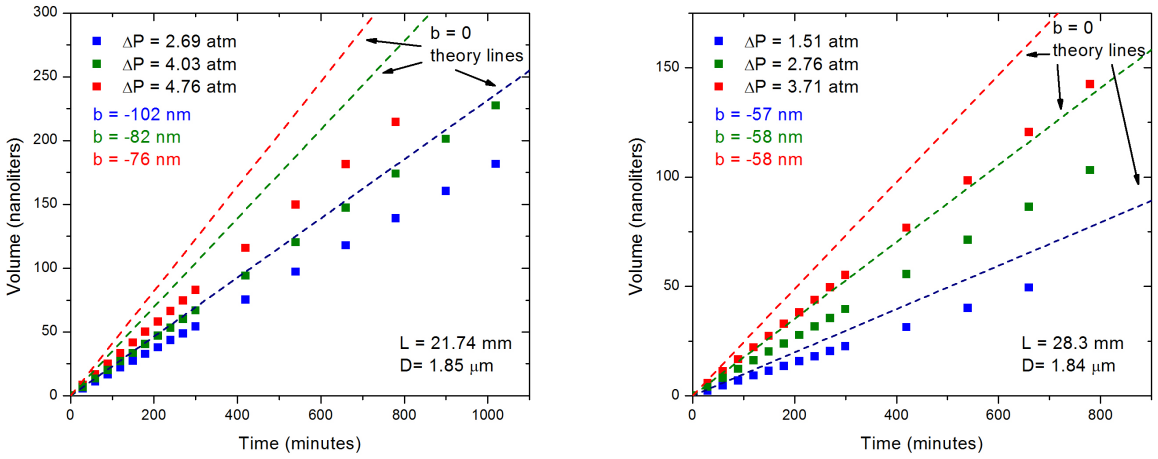

(a) Uncoated 2 μm flow data

(b) PDMS coated 2 μm flow data

Figure 4.3: Flow runs through 2 μm diameter, uncoated and PDMS coated tubes. The difference in measured slip length between uncoated and PDMS coated tubes was 29 nm, which was roughly the same as the range of slip lengths measured in a single tube. It can be concluded that the flows are indistinguishable within a slip length of 30 nm.

4.3 200 nm Data

Reducing the diameter by an order of magnitude from 2 μm to 200 nm decreases flow rates by a factor of 10,000. This is offset partially by increased driving pressure drops that range from 20 to 50 atm. The resultant flow rates are typically on the order of nanoliters per day. The main consequence is longer flow runs, taking usually 2 to 5 days. Considering a single tube may be used for 5 or 6 flow runs, several weeks can be spent on a single tube. Data from the longest flow run performed is shown in Figure 4.4. The data was taken over 5.5 days in an uncoated tube, and resulted in a calculated slip length of -1.2 nm. The inner diameter of the nanotube was measured via SEM.

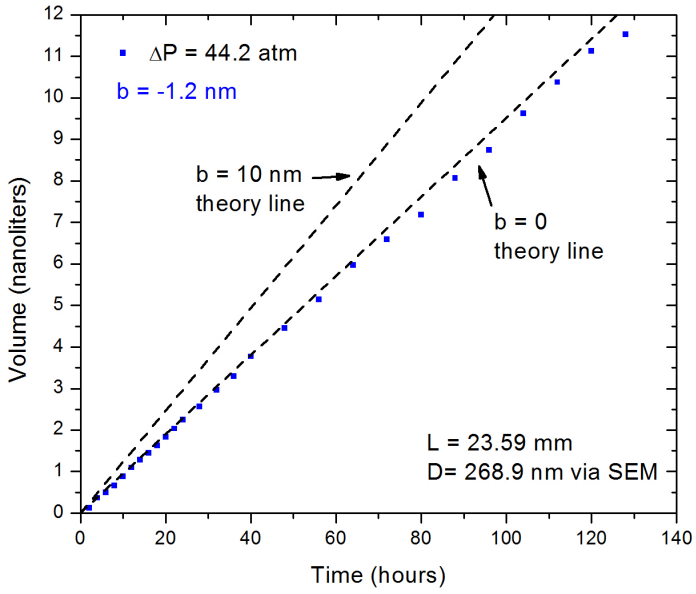

Figure 4.4: The longest single flow run performed in this experiment, lasting 5.5 days and reaching a final drop volume of 12.3 nanoliters. Data was taken for a 23.59 mm long, 268.9 nm diameter uncoated tube with a pressure drop of 44.2 atm. The calculated slip length was calculated to be -1.2 nm.

The data shown in Figure 4.5 of uncoated and PDMS coated 200 nm diameter tubes exhibits the best slip length measurement sensitivity. The uncoated data follows no-slip theory exceptionally well, showing single nanometer slip lengths. The PDMS coated data also follows no-slip theory very well, while showing negative slip lengths between 4 and 5 nm. The difference between the coated and uncoated slip lengths can be attributed to the thickness of the PDMS coating, which was estimated to be less than 2 nm. The two flows are indistinguishable within a slip length of 3 nm.

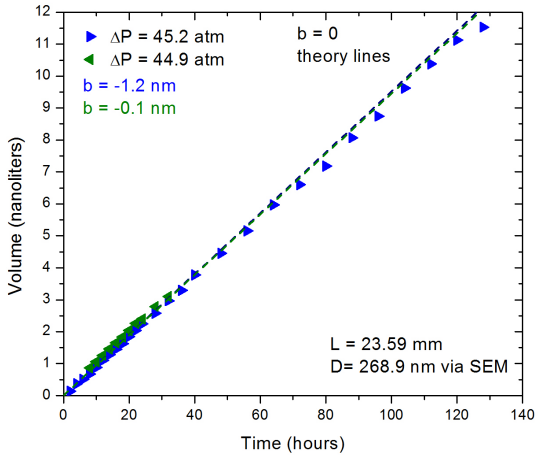

(a) Uncoated 200 nm flow data

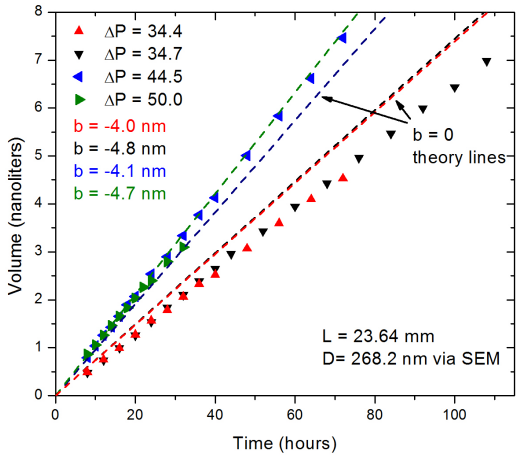

(b) PDMS coated 200 nm flow data

Figure 4.5: Flow runs through 200 nm diameter, uncoated and PDMS coated tubes. The uncoated data agrees very well with no-slip theory, with small slip lengths on the order of 1 nm. The PDMS coated data also agress well with no-slip theory with small, negative slip lengths between 4 and 5 nanometers. The difference between the coated and uncoated data can be explained by the thickness of the PDMS coating, which was estimated to be less than 2 nm. It can still be stated with certainty that the flows are indistinguishable within a slip length of 3 nm.

Chapter 5

Conclusion

Flow rate and slip length were measured in uncoated (hydrophilic) and PDMS coated (hydrophobic) single tubes of diameter 10 μm, 2 μm, and 200 nm. The flow experiments using the 10 μm diameter tubes showed that the flow through the hydrophilic and hydrophobic tubes followed the Hagen-Poiseuille equation and were indistinguishable within a slip length of 100 nm. They also showed no relation between the measured slip length and driving pressure. The 2 μm flow experiments showed negative slip values for both the uncoated and PDMS coated tubes that were indistinguishable within a slip length of 30 nm. The calibration method was changed for the 200 nm tubes, where the flow experiments showed slip values less than 5 nm. The uncoated and coated flows were indistinguishable within a slip length of 3 nm, part of which maybe be due to the thickness of the hydrophobic coating itself. The results of the experiments support the no-slip boundary condition to the limits of the experimental sensitivity. It suggests that reports of greatly enhanced flows due to hydrophobicity may have been caused by experimental error. There are still other possible contributions for slip, such as nanobubbles, that need to be investigated to determine the correct boundary condition.

The method used to measure flows through single nanotubes can be further extended beyond 200 nm diameter tubes, but is only currently limited by finding a supplier or other

way to fabricate said tubes. Current work attempts to tune the cyclohexane:PDMS ratio in order to control the coating thickness to construct a smaller pipe.

Bibliography

[1] B. Bhushan. Biomimetics inspired surfaces for drag reduction and oleophobicity/philicity. *Beilstein journal of nanotechnology*, 2:66–84, Jan. 2011.

[2] F. P. Bretherton. The motion of long bubbles in tubes. *Journal of Fluid Mechanics*, 10(02):166, Mar. 2006.

[3] D. Byun, J. Kim, H. S. Ko, and H. C. Park. Direct measurement of slip flows in superhydrophobic microchannels with transverse grooves. *Physics of Fluids*, 20(11):113601, Nov. 2008.

[4] J.-D. Chen. Measuring the film thickness surrounding a bubble inside a capillary. *Journal of Colloid and Interface Science*, 109(2):341–349, Feb. 1986.

[5] C.-H. Choi, K. J. A. Westin, and K. S. Breuer. Apparent slip flows in hydrophilic and hydrophobic microchannels. *Physics of Fluids*, 15(10):2897, Sept. 2003.

[6] N. Churaev, V. Sobolev, and A. Somov. Slippage of liquids over lyophobic solid surfaces. *Journal of Colloid and Interface Science*, 97(2):574–581, Feb. 1984.

[7] S. Howorka and Z. Siwy. Nanopore analytics: sensing of single molecules. *Chemical Society Reviews*, 38(8):2360, July 2009.

[8] M.-H. Jung and H.-S. Choi. Characterization of octadecyltrichlorosilane self-assembled monolayers on silicon (100) surface. *Korean Journal of Chemical Engineering*, 26(6):1778–1784, Feb. 2010.

[9] G. Lin and A. P. Lee. Microfluidics: an emerging technology for food and health science. *Annals of the New York Academy of Sciences*, 1190:186–92, Mar. 2010.

[10] H. Liu, J. He, J. Tang, H. Liu, P. Pang, D. Cao, P. Krstic, S. Joseph, S. Lindsay, and C. Nuckolls. Translocation of single-stranded DNA through single-walled carbon nanotubes. *Science (New York, N.Y.)*, 327(5961):64–7, Jan. 2010.

[11] M. Majumder, N. Chopra, and B. J. Hinds. Mass transport through carbon nanotube membranes in three different regimes: ionic diffusion and gas and liquid flow. *ACS nano*, 5(5):3867–77, May 2011.

[12] R. Rusconi, S. Lecuyer, L. Guglielmini, and H. A. Stone. Laminar flow around corners triggers the formation of biofilm streamers. *Journal of the Royal Society, Interface / the Royal Society*, 7(50):1293–9, sep 2010.

[13] D. Schaeffel, S. Yordanov, M. Schmelzeisen, T. Yamamoto, M. Kappl, R. Schmitz, B. Dünweg, H.-J. Butt, and K. Koynov. Hydrodynamic boundary condition of water on hydrophobic surfaces. *Physical review. E, Statistical, nonlinear, and soft matter physics*, 87(5):051001, May 2013.

[14] Z. Siwy, P. Apel, D. Baur, D. D. Dobrev, Y. E. Korchev, R. Neumann, R. Spohr, C. Trautmann, and K.-O. Voss. Preparation of synthetic nanopores with transport

properties analogous to biological channels. *Surface Science*, 532-535:1061–1066, June 2003.

[15] D. C. Tretheway and C. D. Meinhart. Apparent fluid slip at hydrophobic microchannel walls. *Physics of Fluids*, 14(3):L9, Mar. 2002.

[16] A. E. Velasco, S. G. Friedman, M. Pevarnik, Z. S. Siwy, and P. Taborek. Pressure-driven flow through a single nanopore. *Physical review. E, Statistical, nonlinear, and soft matter physics*, 86(2 Pt 2):025302, Aug. 2012.

[17] J. Wu, K. S. Paudel, C. Strasinger, D. Hammell, A. L. Stinchcomb, and B. J. Hinds. Programmable transdermal drug delivery of nicotine using carbon nanotube membranes. *Proceedings of the National Academy of Sciences of the United States of America*, 107(26):11698–702, June 2010.